Coalescence of Crystalline Microdomains Driven by Postannealing in a Block Copolymer Blend

Yen-Yu Huang,[†] Hsin-Lung Chen,*[,†] Hsiu-Chun Li,[†] Tsang-Lang Lin,[‡] and J. S. Lin[§]

Department of Chemical Engineering, National Tsing Hua University, Hsin-Chu, Taiwan 30013, R.O.C.; Department of Engineering and System Science, National Tsing Hua University, Hsin-Chu, Taiwan 30013, R.O.C.; and Solid State Division, Oak Ridge National Laboratory, Oak Ridge, Tennessee 37831

Received August 13, 2002

Introduction. Crystalline−amorphous diblock copolymer (C-*b*-A) and its blend with the corresponding homopolymer (C-*b*-A/A) form a special class of material exhibiting two self-organizing mechanisms associated with crystallization and interblock incompatibility. Microphase separation caused by interblock incompatibility tends to form a series of long-range ordered microdomains (e.g., lamellae, cylinder, or sphere) depending upon the composition of the constituting components.[1−9] Crystallization, on the other hand, is prone to create a lamellar morphology consisting of alternating crystalline and amorphous layers with large lateral dimensions.

We consider the case where C block forms microdomains in the melt and the crystallization temperature (T_c) lies above the glass transition temperature of A block (T_g^A), i.e., $T_g^A < T_c < T_{ODT}$; the long-range order and geometric characteristics of microdomains in this case may be perturbed by crystallization because the amorphous matrix remains soft at T_c.[10−20] The extent of structural perturbation is governed by the interplay between the driving force of crystallization and that stabilizing the melt mesophase.[16,19,21] For instance, formation of high crystallinity may deform the (cylindrical or spherical) microdomains significantly (into lamellar shape), which then causes unfavorable perturbations in interfacial tension as well as the conformational entropy of coronal A block chains under the constraint of melt incompressibility. In this case, the system may be resistant to any perturbation in melt structure, and hence C blocks crystallize under the constraint of the prescribed domain geometry leading to lower crystallinity (compared with that in the corresponding homopolymer), because C segments near the domain interface cannot crystallize to largely maintain the interfacial curvature. On the other extreme, when the free energy reduction due to formation of large lamellar crystals overwhelms the unfavorable contribution arising from melt structure perturbation, crystallization would erase the melt mesophase and transform it into a lamellar morphology through extended crystal growth. Nevertheless, such a morphological transformation is not guaranteed even if lamellar morphology is predicted to be the equilibrium structure, since the activation barriers to the transformation process are also critical. We expect those barriers to increase with increasing spatial restriction to extended crystal growth, namely, spherical morphology exerts a higher barrier than cylindrical structure; as a result, the observed crystalline morphology could be stable (a consequence of minimization in free energy relevant to crystallization and microphase separation) or metastable (a kinetically controlled structure).

In the microphase-separated melt consisting of cylindrical or spherical microdomains, coalescence or welding of individual domains must occur on the way to the formation of large crystalline lamellae. Nojima et al. reported the formation of crystalline lamellar structure in a sphere-forming polycaprolactone-*block*-polybutadiene (PCL-*b*-PB) upon PCL crystallization.[12] A recent study by Loo et al. showed that the spherical microdomains formed by polyethylenene block in polyethylene-*block*-poly(styrene-*r*-ethylene-*r*-butene) (E/SEB) did not weld into large lamellae upon slow crystallization; alternatively, disk- or rodlike domains were formed through rather local coalescence.[19] The detailed mechanism of "crystallization-induced microdomain coalescence" has not been resolved so far. It has been suggested that sufficient deformation of microdomain interface by the growing crystal could allow the interfaces of the neighboring domains to meet, thereby permitting the crystal growth fronts in the crystallizing domains to intrude into the nearby molten domains easily and consequently leads to extended crystal growth.[19] Another "dissociation/association" mechanism proposed by Nojima et al. asserts that the driving force of crystal growth can pull C blocks out of the molten domains; these block chains then diffuse across the matrix and eventually add onto the growing crystal surface that appeared in the crystallizing domains, leading to extended crystal growth from an originally nanoscaled domain.[12]

Among those instances of microdomain welding reported so far, the processes took place during the crystallization, wherein the block chains in the otherwise molten domains have large mobility (compared with the crystalline chains) to participate in the diffusion or conformational rearrangement necessary for creating domain coalescence. In this study, we demonstrate that the welding of microdomains can also be driven through a postannealing treatment, where the crystalline samples (having reached the saturated crystallinity at T_c) are annealed at temperatures significantly higher than T_c but lower than the melting points. Since nearly all domains remain semicrystalline during the annealing, this coalescence process is distinguished from that found in the crystallization process or that associated with the order−order transition from spherical to cylindrical domains in block copolymer melt.[22−23]

Experimental Section. The system under study is the blend of a poly(ethylene oxide)-*block*-polybutadiene (PEO-*b*-PB) and a PB homopolymer. The PEO-*b*-PB with the polydispersity index (M_w/M_n) = 1.04 was synthesized by sequential anionic polymerization of butadiene and ethylene oxide (Polymer Source, Inc.). M_n of the PEO and PB blocks was 6000 and 20 400, respectively. This diblock was mixed with a PB homopolymer (with M_n = 1000 and M_w/M_n = 1.04) to yield a wet-brush PEO-*b*-PB/PB blend with the overall vol-

[†] Department of Chemical Engineering, National Tsing Hua University.
[‡] Department of Engineering and System Science, National Tsing Hua University.
[§] Oak Ridge National Laboratory.
* To whom correspondence should be addressed.

10.1021/ma0213201 CCC: $25.00
Published on Web 12/19/2002

Table 1. Crystallinities (X_c) and Melting Points (T_m) of As-Crystallized and Annealed PEO-*b*-PB/PB Blend with $f_{PEO} = 0.17$

crystallization or annealing condition	X_c[a]	T_m (°C)[b]
as-crystallized at −30 °C	0.66	52
as-crystallized at −50 °C	0.65	50
annealed at 38 °C after −30 °C crystallization	0.80	56
annealed at 41 °C after −30 °C crystallization	0.79	55
annealed at 38 °C after −50 °C crystallization	0.81	57
annealed at 41 °C after −50 °C crystallization	0.80	55

[a] X_c was calculated from the enthalpy of melting (Δh_f) measured by DSC, i.e., $X_c = \Delta h_f/(\Delta h_f{}^0 w_{PEO})$, with $\Delta h_f{}^0$ (=200 J/g) and w_{PEO} being the bulk enthalpy of melting and weight fraction of PEO, respectively. [b] The uncertainty of T_m is about ±1 °C.

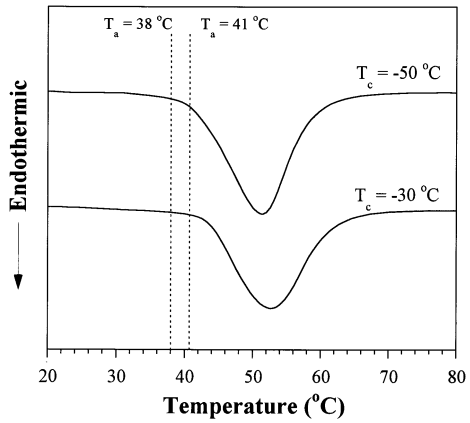

Figure 1. DSC melting curves of PEO-*b*-PB/PB blend ($f_{PEO} = 0.17$) recorded after crystallizations at −30 and −50 °C. The locations of the annealing temperatures chosen (i.e., $T_a = 38$ and 41 °C) are indicated by the dashed lines. Both T_a's are seen to situate near the onsets of melting.

ume fraction of PEO, $f_{PEO} = 0.17$ (the amount of PB homopolymer in the blend was 12 wt %). The blending was conducted by solution mixing using toluene as the cosolvent, followed by removing the solvent in vacuo at 80 °C. The resultant microphase-separated blend was found to consist of bcc packed PEO spheres in the melt.[20]

PEO-*b*-PB/PB blend was isothermally crystallized at −30 or −50 °C to reach the saturated crystallinities at the prescribed T_c's prior to the postannealing treatment. For the isothermal crystallization, the sample was quenched directly from 85 °C ($T_{ODT} > 85$ °C $> T_m^{PEO}$) to T_c followed by crystallization at T_c for 4 h. The crystallinities (normalized by the weight fraction of PEO) of the as-crystallized samples are tabulated in Table 1. Postannealing was conducted by storing the as-crystallized samples in an oven equilibrated at $T_a = 38$ or 41 °C for 96 h. The DSC melting curves of the blend crystallized at −30 and −50 °C are shown in Figure 1. It can be seen that both T_a's are located near the onsets of melting; therefore, PEO domains remain predominantly semicrystalline during the annealing process.

SAXS characterizations of all samples were conducted at room temperature. The SAXS apparatus consisted of an 18 kW rotating-anode X-ray generator operated at 40 kV × 200 mA (Rigaku), a graphite crystal for incident beam monochromatization, and a two-dimensional position-sensitive detector (ORDELA model 2201X, Oak Ridge Detector Laboratory Inc.). The intensity profiles were output as the plot of scattering intensity (I) vs scattering vector, $q = (4\pi/\lambda)\sin(\theta/2)$ (θ = scattering angle). Details of the SAXS setup have been described elsewhere.[18]

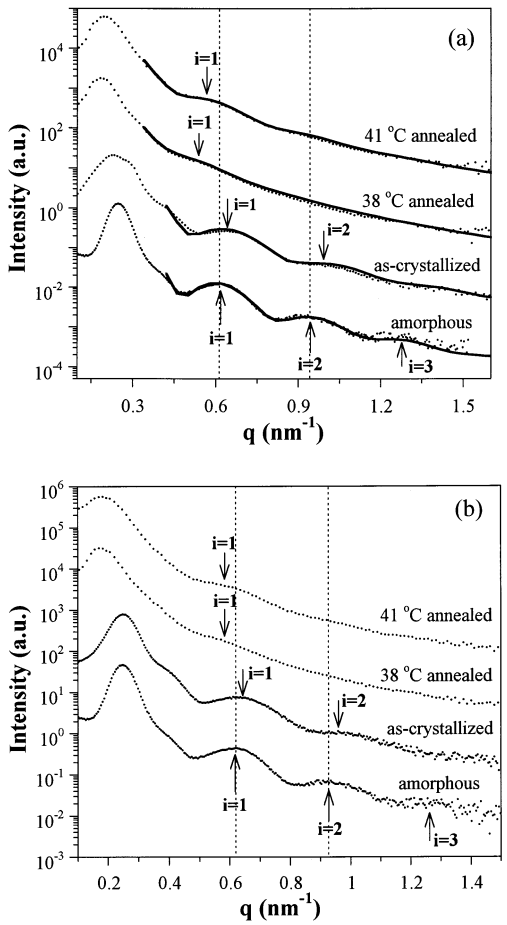

Figure 2. SAXS profiles of the amorphous, as-crystallized, and annealed samples of PEO-*b*-PB/PB blend ($f_{PEO} = 0.17$). The crystallization temperatures are (a) −30 °C and (b) −50 °C. The scattering maxima denoted by "$i = n$" ($n = 1, 2, 3, ...$) are the form factor peaks. Both lattice and form factor scatterings are significantly perturbed after the as-crystallized samples have been subjected to postannealing. The solid curves in (a) are the profiles calculated using elliptic form factor. The average dimensions obtained are listed in Table 2.

Observation of real-space morphology was conducted at room temperature by a JEOL JEM-2000FXZ transmission electron microscope operated at 120 kV. The film specimens were microtomed at −90 °C, using a Reichert Ultracut E low-temperature sectioning system. The ultrathin sections were stained with the vapor of 1% OsO_4(aq) for 1 h.

Results and Discussion. Figure 2 displays the SAXS profiles of the amorphous, as-crystallized, and annealed samples. The scattering maxima denoted by "$i = n$" ($n = 1, 2, 3, ...$) correspond to the form factor peaks associated with the scattering from isolated microdomains.[18,20] Form factor scattering depends on the geometric characteristics of the microdomains, including the shape, the average dimension, and the dimension distribution. The samples as-crystallized at both T_c's exhibit primary lattice peaks at approximately the same position as that of the amorphous sample, but the peaks are broader. The corresponding form factor peaks move slightly to higher q upon the crystallization. As has been discussed in our previous study,[20] the observed shifts in form factor maxima cannot be simply attributed to volume contraction of spherical microdomains, because, although the observed profiles could be fitted by spherical form factor, the radius obtained

Table 2. Results of the Fit by Elliptic Form Factor for PEO-*b*-PB/PB Blend ($f_{PEO} = 0.17$) Subjected to Crystallization at −30 °C and Postannealing

sample	$\langle a \rangle$ (nm)	$\langle b \rangle$ (nm)	σ_a (nm)[a]	σ_b (nm)[a]
amorphous	9.5	9.3	0.8	1.0
as-crystallized	11.0	8.2	1.0	0.7
annealed at 38 °C	30.0	9.4	3.0	1.6
annealed at 41 °C	30.0	9.0	3.0	1.0

[a] σ_a and σ_b are the standard deviation of a and b; Gaussian distributions were assumed.

from the fit yielded the domain density that was higher than the crystal density of PEO. The observed form factor profiles could be equally fitted by the elliptic form factor, which yielded reasonable density for the semicrystalline domains.[20] The dimensions of the ellipsoid considered was characterized by a and b, with the axis of a being the rotating axis of the ellipse.[24] For demonstration, the average dimensions of the ellipsoidal domains, $\langle a \rangle$ and $\langle b \rangle$, deduced from the form factor fit are listed in Table 2 for the sample crystallized at −30 °C. It can be seen that the original molten spheres with radius of ca. 9.4 nm deformed slightly into ellipsoid-like domains with aspect ratio $\langle a \rangle / \langle b \rangle = 1.34$.

As shown in Figure 2, both lattice and form factor scatterings are significantly perturbed after the as-crystallized samples have been subjected to postannealing at 38 and 41 °C. The primary lattice peak shifts from 0.25 to ca. 0.18 nm^{-1}, signaling a strong perturbation in the long-range order. The geometric characteristics of the crystalline domains have also been affected because the form factor maxima also move to lower q and smear out after the annealing.

Since it is hard to tell from the observed scattering profiles as to the type of structure formed after the annealing treatment, the TEM experiment was conducted to observe the morphology in real space. Figure 3a−c presents a series of TEM micrographs of the as-crystallized and annealed samples. The slightly ellipsoidal domains found in the as-crystallized sample are seen to transform into highly elongated prolates or rodlike domains after the annealing. These rods are of ca. 30−70 nm in length and ca. 20 nm in diameter, and their orientations are rather random with some arranged flat-on and some side-on. Since the volume of individual rods exceeds that of a single microdomain found in the as-crystallized sample, the rodlike domains must have been formed through coalescence of the crystalline domains in the annealing process, where approximately two or three domains weld into one rod.

The SAXS form factor profiles observed for the annealed samples can be fitted well by the elliptic form factor using the dimensions corresponding to highly elongated prolates, as demonstrated by the solid curves in Figure 2a. The average dimensions derived from the fits are shown in Table 2. Although $\langle a \rangle$ and $\langle b \rangle$ thus obtained agree with the half-length and radius of the rods estimated from TEM, respectively, it should be noted that the positions of the form factor maxima are largely determined by the value of $\langle b \rangle$ (i.e., not sensitive to the value of $\langle a \rangle$) once $\langle a \rangle$ exceeds ca. 12 nm in the present case.

The reason that the primary scattering peak shifts (to lower q) significantly after the annealing can also be understood by considering the morphology observed by TEM. It is known that the primary diffraction peak of bcc packed spheres is associated with the (110) lattice plane.[25] From the TEM micrographs we see a complete loss of bcc order upon transformation into rodlike domains, and the arrangement of rods cannot be represented by any well-defined lattice structure; therefore, upon the annealing, the original (110) peak observed in the amorphous or as-crystallized samples transforms into that characterizing the spatial correlation of the rods and consequently causes the peak shift.

Because PEO blocks in the microdomains remain semicrystalline during the postannealing, the dynamics of domain welding is slow, where the structural perturbation becomes evident (judging from the peak shift in SAXS pattern) only after prolonged treatment (>72 h) at temperatures close to the onset of melting. Both the crystallinity and melting point (T_m) of the annealed samples are higher than those of the as-crystallized counterparts, as shown in Table 1. For homopolymer, the observed T_m is largely determined by the thickness of crystal (l_c), since this temperature corresponds to the equilibrium point between the pure molten state and the metastable crystalline state whose free energy is closely governed by l_c. The scenario becomes more complex in C−A diblocks, in that T_m represents the transition from microphase-separated crystalline state to microphase-separated molten state. The free energies of these two states contain additional contributions from the conformational entropy of C and A blocks and interfacial energy between C and A domains; therefore, the observed T_m depends on these parameters besides crystal thickness.[26] Considering the additional contributions of conformational entropy and interfacial energy, Hong et al. predicted the observed T_m of a PEO-*b*-PB (with PEO block length similar to that of the sample studied here) to pass through a maximum at the "equilibrium crystal thickness".[26] If the crystalline lamellar thickness becomes larger than the limiting value, T_m is reduced as unfavorable stretching of PB chains begins to dominate. In light of such a $T_m - l_c$ dependence, the observed rise in T_m upon postannealing may hence be caused by either crystal thickening or crystal thinning, although, to our knowledge, T_m increase due to crystal thinning has never been observed in C−A diblocks.

The observed domain welding is proposed to stem from further perturbation in microdomain geometry induced by postannealing. Because the composition of the blend ($f_{PEO} = 0.17$) is in the vicinity to that corresponding to the cylindrical−spherical domain transition, moderate perturbation in the geometry of the originally spherical domains may increase the interfacial energy and hence brings about domain coalescence. During the postannealing, further development of crystallinity (from 65 to 80%) and change of crystal dimension through crystal thickening (or thinning) tend to deform PEO domains more; large deviation of domain geometry from sphere may increase the interfacial area between the domains and PB matrix to such an extent that the interfaces of the discrete microdomains become unstable. Domain coalescence then occurs where the microdomains are pulled together by coronal PB blocks through thermal activation.

The microdomain welding appears to be suppressed by decreasing PEO volume fraction in the blend, i.e., by further drifting the composition away from that at the cylindrical−spherical domain transition. Figure 3d displays the TEM micrograph of the blend with $f_{PEO} = 0.13$ subjected to crystallization at −30 °C and then annealing at 38 °C for 96 h. It is apparent that the

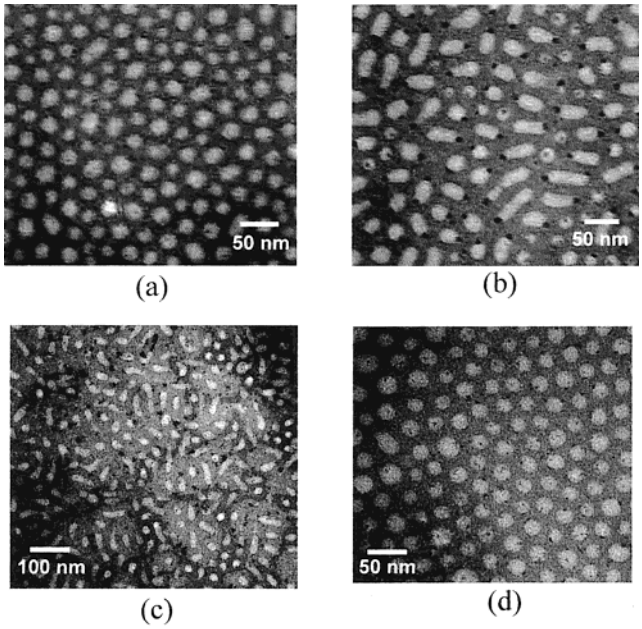

Figure 3. Representative TEM micrographs showing the morphology of the as-crystallized or annealed samples for the blends with $f_{PEO} = 0.17$ and 0.13. The composition and thermal treatment are (a) $f_{PEO} = 0.17$, as-crystallized at −30 °C; (b) $f_{PEO} = 0.17$, annealed at 38 °C after crystallization at −30 °C; (c) $f_{PEO} = 0.17$, annealed at 41 °C after crystallization at −50 °C; and (d) $f_{PEO} = 0.13$, annealed at 38 °C after crystallization at −30 °C.

crystalline domains did not coalesce even though the interdomain distance was similar to that in the blend with $f_{PEO} = 0.17$.

Conclusions. In summary, we have reported the coalescence of crystalline microdomains driven by annealing a PEO-*b*-PB/PB blend at temperatures near the onsets of melting of the as-crystallized samples. Two or three crystalline domains were found to merge into a highly elongated prolate or a rodlike domain through the postannealing. Since nearly all microdomains remained semicrystalline during the treatment, this coalescence process was distinguished from that found in the crystallization process or that associated with the order−order transition from spherical-to-cylindrical domains in block copolymer melt. The driving force for the observed domain welding should be of worthy for further exploration. It is possible that further development of crystallinity and perturbation in crystal dimension through crystal thickening (or thinning) during postannealing introduced enough interfacial deformation to destabilize the microdomain interface and consequently induced domain coalescence to reduce the interfacial tension. It would be of interest to reveal whether such a domain coalescence could occur in other systems such as polyethylene (PE)-based diblock copolymers derived from hydrogenated poly(1,4-butadiene). Unlike PEO, those PE blocks may not undergo crystal thickening on annealing as the equilibrium thickness is dedicated by the branch content. However, the crystallinity may still be enhanced upon annealing, so such a system may be considered for revealing whether further development in crystallinity is the dominant driving force for microdomain coalescence.

Acknowledgment. This work was supported by the National Science Council of R.O.C. under Grant NSC 90-2216-E-007-035 and also in part by the US Department of Energy under Contract DE-AC05-00OR22725 with the Oak Ridge National Laboratory, managed by the UT-Battelle, LLC.

References and Notes

(1) Leibler, L. *Macromolecules* **1980**, *13*, 1602.
(2) Hashimoto, T.; Shibayama, M.; Fujimura, M.; Kawai, H. In *Block Copolymers-Science and Technology*; Meier, D. J., Ed.; Harward Academic Publishers: London, 1983.
(3) Hamley, I. W. *The Physics of Block Copolymers*; Oxford University Press: New York, 1998.
(4) Bates, F. S.; Fredrickson, G. H. *Phys. Today* **1999**, *52*, 32.
(5) Roe, R. J.; Zin, W. C. *Macromolecules* **1984**, *17*, 189.
(6) Hashimoto, T.; Tanaka, H.; Hasegawa, H. *Macromolecules* **1990**, *23*, 4387.
(7) Nojima, S.; Roe, R. J.; Rigby, D.; Han, C. C. *Macromolecules* **1990**, *23*, 4305.
(8) Tanaka, H.; Hasegawa, H.; Hashimoto, T. *Macromolecules* **1991**, *24*, 240.
(9) Winey, K. I.; Thomas, E. L.; Fetters, L. J. *Macromolecules* **1992**, *25*, 2645.
(10) Cohen, R. E.; Cheng, P. L.; Douzinas, K.; Kofinas, P.; Berney, C. V. *Macromolecules* **1990**, *23*, 324.
(11) Nojima, S.; Kato, K.; Yamamoto, S.; Ashida, T. *Macromolecules* **1992**, *25*, 2237.
(12) Nojima, S.; Nakano, H.; Takahashi, Y.; Ashida, T. *Polymer* **1994**, *35*, 3479.
(13) Ryan, A. J.; Hamley, I. W.; Bras, W.; Bates, F. S. *Macromolecules* **1995**, *28*, 3860.
(14) Schnablegger, H.; Rein, D. H.; Rempp, P.; Cohen, R. E. *J. Polym. Eng.* **1996**, *16*, 1.
(15) Nojima, S.; Tanaka, H.; Rohadi, A.; Sasaki, S. *Polymer* **1998**, *39*, 1727.
(16) Zhu, L.; Chen, Y.; Zhang, A.; Calhoun, B. H.; Chun, M.; Quirk, R. P.; Cheng, S. Z. D.; Hsiao, B. S.; Yeh, F.; Hashimoto, T. *Phys. Rev. B* **1999**, *60*, 10022.
(17) Loo, Y.-L.; Register, R. A.; Adamson, D. H. *J. Polym. Sci., Polym. Phys. Ed.* **2000**, *38*, 2564.
(18) Chen, H. L.; Wu, J. C.; Lin, T. L.; Lin, J. S. *Macromolecules* **2001**, *34*, 6936.
(19) Loo, Y.-L.; Register, R. A.; Ryan, A. J. *Macromolecules* **2002**, *35*, 2365.
(20) Chen, H.-L.; Li, H.-C.; Huang, Y.-Y.; Chiu, F.-C. *Macromolecules* **2002**, *35*, 2417.
(21) Quiram, D. J.; Register, R. A.; Marchand, G. R. *Macromolecules* **1997**, *30*, 4551.
(22) Sakurai, S.; Kawada, H.; Hashimoto, T.; Fetters, L. J. *Macromolecules* **1993**, *26*, 5796.
(23) Kimishima, K.; Koga, T.; Hashimoto, T. *Macromolecules* **2000**, *33*, 968.
(24) Feigin, L. A.; Svergun, D. I. *Structure Analysis by Small-Angle X-Ray and Neutron Scattering*; Plenum Press: New York, 1987.
(25) Cullity, B. D.; Stock, S. R *Elements of X-Ray Diffraction*; Prentice Hall: Upper Saddle River, NJ, 2001; Chapter 10.
(26) Hong, S.; Yang, L.; MacKnight, W. J.; Gido, S. P. *Macromolecules* **2001**, *34*, 7009.

MA0213201